Geophys. J. Int. (2008) **172,** 770–778 doi: 10.1111/j.1365-246X.2007.03681.x

The role of shear and tensile failure in dynamically triggered landslides

T. L. Gipprich,[1] R. K. Snieder,[1] R. W. Jibson[2] and W. Kimman[1]

[1] *Center for Wave Phenomena and Department of Geophysics, Colorado School of Mines,* 1500 *Illinois Street, Golden,* CO 80401-1887 *USA. E-mail: rsnieder@mines.edu*

[2] *The United States Geological Survey,* PO Box 25046, *Mail Stop* 966, *Golden,* CO 80225, *USA*

Accepted 2007 November 5. Received 2007 October 25; in original form 2007 June 13

SUMMARY

Dynamic stresses generated by earthquakes can trigger landslides. Current methods of landslide analysis such as pseudo-static analysis and Newmark's method focus on the effects of earthquake accelerations on the landslide mass to characterize dynamic landslide behaviour. One limitation of these methods is their use Mohr–Coulomb failure criteria, which only accounts for shear failure, but the role of tensile failure is not accounted for. We develop a limit-equilibrium model to investigate the dynamic stresses generated by a given ground motion due to a plane wave and use this model to assess the role of shear and tensile failure in the initiation of slope instability. We do so by incorporating a modified Griffith failure envelope, which combines shear and tensile failure into a single criterion. Tests of dynamic stresses in both homogeneous and layered slopes demonstrate that two modes of failure exist, tensile failure in the uppermost meters of a slope and shear failure at greater depth. Further, we derive equations that express the dynamic stress in the near-surface in the acceleration measured at the surface. These equations are used to approximately define the depth range for each mechanism of failure. The depths at which these failure mechanisms occur suggest that shear and tensile failure might collaborate in generating slope failure.

Key words: Site effects; Wave propagation.

1 INTRODUCTION

Most moderate to large earthquakes trigger landslides. While current methods used to model these landslides are useful, they are based solely on shear failure and thus fail to account for the role of tensile stresses in the failure process. The most commonly used current methods include pseudo-static analysis and Newmark's method. These methods are based on modelling the limit-equilibrium condition in terms of the factor of safety (FS), which describes the stability of a slope as the ratio of resisting to driving forces (Terzaghi 1950). When this ratio is greater than 1.0, the slope is stable; when it is less than 1.0, the slope is unstable. Pseudo-static analysis is a limit-equilibrium analysis where the ground acceleration from an earthquake is computed as an additional static body force acting on the slope. A factor-of-safety analysis based on force equilibrium is carried out for different acceleration values to determine the critical value that reduces the factor of safety to 1.0.

Newmark's method goes further by estimating the permanent slope displacement caused by an earthquake (Newmark 1965). The critical acceleration a slope can withstand during an earthquake is given by Jibson *et al.* (2000)

$$a_c = (FS - 1)g \sin(\theta), \tag{1}$$

where g is gravitational acceleration and θ the slope angle. (We show a table with the employed notation at the end of the paper.) An acceleration larger than this value initiates sliding. In Newmark's method one estimates the permanent displacement by double-integrating the parts of an earthquake acceleration-time history that exceed the critical acceleration (Jibson 1993; Jibson *et al.* 2000). Newmark's method models a landslide as a rigid friction block sliding without internal deformation on an inclined plane. Therefore, it is most appropriately applied to landslides in stiff material that slide on a basal shear surface. Newmark's method does not work very well for deep landslides in soft material (e.g. clay), where internal deformation occurs and modifies the shaking response (Rathje & Bray 1999, Rathje & Bray 2000). There is evidence from field observations (Harp *et al.* 1981) and laboratory studies (Sitar & Clough 1983) of tensile failure in earthquake-triggered landslides, especially in relatively shallow failures in weak, brittle materials (so-called weakly cemented soils).

While pseudo-static analysis and Newmark's method focus on earthquake-induced accelerations to account for shear failure, we focus on the dynamic stress state generated from a given ground motion and how this causes both shear and tensile failure at the initiation of slope instability. Our work accounts both for shear failure and tensile failure, and is more general than Newmark's method because it accounts for the stress throughout the subsurface rather than describing the near-surface as a rigid block. Post-failure

deformation of a slope is not accounted for in our work because the employed linearized stress–strain relation does not accommodate material properties of material that has failed.

First, we describe the static and dynamic stresses in a dry, infinite slope and the failure criterion used to define failure. The infinite slope model is a commonly used idealization in slope stability studies for situations where the length parallel to the slope is much greater than the depth of the slide mass. This model is applicable when any given element on the slope is not strongly affected by up or down slope end-effects. By testing several wave-propagation scenarios, we show that two modes of failure develop in homogeneous and layered slopes. For the conditions modelled, tensile failure due to dynamic stresses occurs in the upper 2 m of a slope, while shear failure takes place at greater depth within the upper 10 m.

To further understand the regions of shear and tensile failure in a slope, we derive dynamic stress equations that relate dynamic stresses in the near-surface to the acceleration at the surface. By explicitly specifying the peak ground acceleration (PGA) in this analysis, these equations produce dynamic stresses as a function of depth that help predict the depth ranges for each failure mechanism. Shear and tensile failure is predicted to occur at different depths, and we show how the two failure mechanisms collaborate to cause slope failure. Because this model is based on a limit-equilibrium method, we cannot model post-failure deformation of a slope, but our analysis elucidates the roles of tensile and shear failure.

2 STATIC STRESS IN A SLOPE

We consider a one-dimensional (1-D) static stress model to compute the initial static stress-state of a slope. For the dynamic stress we use a 2-D model, hence the dynamic stress is a function of two space coordinates. The coordinate system used throughout this study (Fig. 1) defines the x-direction as parallel to the surface of the slope and depth, z, normal to the slope.

We use a simple static stress model for near-surface stresses caused by gravity (Savage & Swolfs 1992). In this model, the near-surface is assumed to be linearly elastic and the infinite, planar slope is laterally constrained so material cannot expand in the direction parallel to the slope (Mello & Pratson 1999). Because of translational invariance of an infinite slope, stress does not depend on the downslope location. This does not imply that there is no displacement along the slope, but the x-derivatives of the displacement vanish and do not contribute to the static stress.

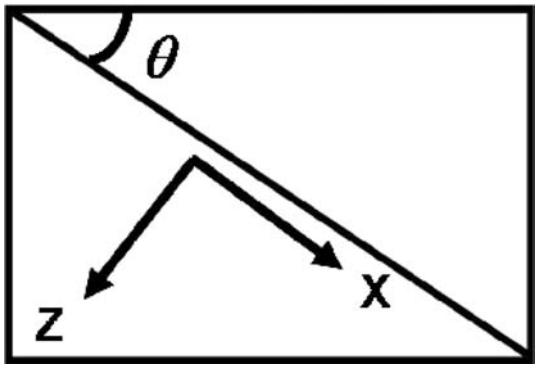

Figure 1. Coordinate system used in this work, where θ is the slope angle. The x-direction, or downslope direction, is parallel to the slope and the z-coordinate measures the distance normal to the slope.

The equations of stress for this model are (Jaeger & Cook 1976; Savage & Swolfs 1992)

$$\sigma_{xx}^{\text{static}} = \frac{\lambda}{\lambda + 2\mu} \rho g z \cos(\theta), \tag{2}$$

$$\sigma_{zz}^{\text{static}} = \rho g z \cos(\theta), \tag{3}$$

$$\sigma_{xz}^{\text{static}} = \rho g z \sin(\theta), \tag{4}$$

where λ and μ are Lamé elastic constants, ρ is the density, g is gravitational acceleration, and θ is the slope angle. Normal stresses are considered positive in compression and negative in tension. The stress components are for the coordinate with the x-axis parallel to the slope and the z-axis perpendicular to the slope. This means, for example, that σ_{xx} is the compressive stress parallel to the slope.

For a finite slope the stress varies along the slope. Such a slope is weakest in the area of maximum deviatoric stress. Because of stress concentrations near the endpoints of such a slope the deviatoric stress in a finite slope is, in general, larger than in the infinite slope model used in our study. For this reason, failure may occur in a finite slope for a smaller peak ground acceleration than is predicted for our model. The goal of this study is to understand the physics of different failure mechanisms for landslides rather than a quantitative prediction for which ground motion failure occurs. For such a study one would also need to account for the focusing of wave energy by realistic topography.

Before modelling the plane-wave propagation through a slope, we carry out a static slope-stability analysis to find whether the unperturbed static slope is stable. We do so by increasing the slope angle to see at which point a slope fails. In this way, we can define a slope that is stable under static conditions, but that can fail dynamically.

3 DYNAMIC STRESSES DUE TO A PLANE WAVE INCIDENT ON A SLOPE

We compute the dynamic stresses created from a plane wave incident on a slope using a finite element wave equation code. We use second-order equations of motion that solve for displacement, u_x and u_z (Haney 2004). This 2-D model allows us to account for extensional strain associated with wave propagation. Since we study tensile failure, we limit the analysis to *P–SV* waves (Aki & Richards 2002). The elements used in the finite element span a depth of 1 m in the z-direction each. Because of the linear interpolation within the elements the variations of the wave field within the elements is also known.

Solutions of the form $F = F(t - px, z)$ describe a plane wave moving in the x-direction in time t, with a slowness p along the slope. In a medium where properties vary with depth only, p is constant and known as the ray parameter of the wave incident on the surface (Aki & Richards 2002)

$$p = \frac{\sin(i_p)}{v_p} = \frac{\sin(i_s)}{v_s}, \tag{5}$$

where i_p and i_s are the incidence angles that P and S waves make with the normal axis of the slope, and v_p and v_s are the P- and S-wave velocities, respectively. For this solution the downslope derivative is related to the time derivative by

$$\frac{\partial F(t - px, z)}{\partial x} = -p \frac{\partial F(t - px, z)}{\partial t}. \tag{6}$$

The finite element code produces displacement, velocity and acceleration as well as the stress components, $\sigma_{xx}^{\text{dynamic}}$, $\sigma_{zz}^{\text{dynamic}}$ and

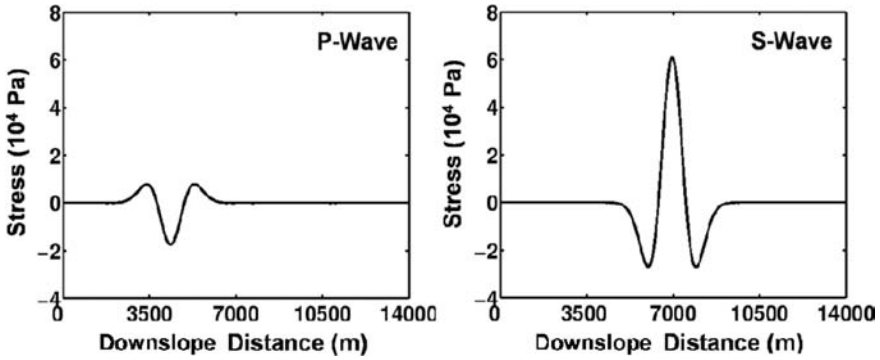

Figure 2. $\sigma_{xx}^{\text{dynamic}}$ component of stress for both 30° incident *P* and *S* waves at the surface of a slope for a PGA of 0.1 g. The *S* wave produces larger stress at the surface than does the *P* wave.

$\sigma_{xz}^{\text{dynamic}}$ for a given incoming wave. At the free surface, the tractions vanish (Aki & Richards 2002):

$$\sigma_{zz}^{\text{dynamic}}(z=0) = \sigma_{xz}^{\text{dynamic}}(z=0) = 0. \tag{7}$$

Once the dynamic stresses are known, the total stress state is given by the sum of the dynamic and static stress:

$$\sigma_{ij}^{\text{total}} = \sigma_{ij}^{\text{static}} + \sigma_{ij}^{\text{dynamic}}. \tag{8}$$

Failure depends on the peak ground acceleration (PGA) of the incoming wave, and for each slope, there exists a PGA that initiates failure at one location for a given instant in time. As that PGA value increases, the values of the dynamic stresses also increase and the slope fails, but the employed linear model does not account for post-failure behaviour. A PGA between 0.1*g* and 1.0*g* is common during earthquakes (Jibson 1993). We normalize the wavefield in all simulations such that the PGA is equal to 0.1*g*. The incoming wave used in this analysis has a peak frequency of 1.0 Hz, which is near the centre of the range of frequencies normally associated with earthquake-triggered landslides (Jibson *et al.* 2004; Bray & Rathje 1998).

We analyse both *P* and *S* waves. When both waves are normalized to the same PGA as described above, the dynamic stresses produced by the *S* wave are larger at the surface of the slope than for the *P* wave. Fig. 2 is a comparison of the $\sigma_{xx}^{\text{dynamic}}$ component of stress for *P* and *S* waves with a 30° angle of incidence that are normalized to a PGA of 0.1 g. This example shows that for a given PGA the stress is greater at the surface for the *S* wave than for the *P* wave. As the angle of incidence changes, the stress components also change, which may influence the initiation of slope failure. Regardless of the type of incident wave, for a variety of incidence and slope angles, both shear and tensile failure can occur. In this paper, we show examples of slope failure due to dynamic stresses generated by a 30° incident wave.

4 FAILURE CRITERIA

When analysing static slope stability, a discrepancy arises between the static stress model given by expressions (2)–(4) and other traditional models. In a Mohr–Coulomb slope-stability analysis, the limiting-equilibrium condition of an infinite slope is expressed as a factor-of-safety against failure along a surface parallel to the slope. The model discrepancy is best illustrated in the simplest condition—a dry, cohesionless slope—in which the FS is simply

$$FS = \frac{\tan(\phi)}{\tan(\theta)}, \tag{9}$$

where ϕ is the internal angle of friction and θ is the slope angle. Slope instability occurs when ϕ is equal to θ, or when $FS = 1.0$. In contrast to this, the static stress state defined by eqs (2)–(4) for a plane infinite slope, produces failure at a critical angle, θ_c, that is smaller than the internal angle of friction ϕ. This also is the case when cohesion is included in the static stress model.

Although the source of the discrepancy between the two models is not completely clear, it likely relates to our assumption of a laterally constrained, infinite slope. In such a model, the slope-parallel derivatives vanish, and the material cannot expand laterally. This stress model is widely used in soil mechanics, and we work with the equations in this model to understand how changes in the total stress state due to dynamic stresses lead to slope failure.

When a wave passes through a slope, dynamic stresses are generated that can cause certain locations within the slope to fail. To understand the potential for shear failure, a Mohr–Coulomb failure analysis is commonly employed which tests whether stress exceeds strength. The shear strength (τ) of a failure surface in dry conditions is characterized by the Mohr–Coulomb failure criterion (e.g. Bourne & Willemse 2001),

$$\tau = c + \sigma \tan(\phi), \tag{10}$$

where c is cohesion of a material and σ is the normal stress. In this analysis, we consider sands having cohesions of 0–20 kPa (Selby 1993; Middleton & Wilcock 1994) and friction angles of 30°–34° (Selby 1993; Das 1997). Fig. 3 shows a Mohr circle and Mohr–Coulomb failure envelope. Shear failure takes place at the critical angle, $\theta_c = (90^\circ + \phi)/2$ (Das 1997). A post-failure state of stress represented by a Mohr circle lying outside of the envelope is not accounted for by our dynamic model.

To determine the locations of both shear and tensile failure of cohesive soils, we incorporate the Griffith failure criterion to account for tensional failure. Thin, microscopic cracks dominate the tensile strength and propagate under stress conditions defined by the Griffith criterion (Bourne & Willemse 2001),

$$\tau^2 = 2c\sigma + c^2. \tag{11}$$

A modification of this failure envelope has been introduced by Brace (1960), who defines a single stress criterion that includes both shear and tensile failure (Fig. 4). For negative values of normal stress, the curved part of the envelope is defined by eq. (11). For positive values of normal stress, the envelope is defined by eq. (10). The region of the failure envelope first encountered by the Mohr circle defines the type of failure of the stress state (Bourne & Willemse 2001). As shown in Fig. 4, we use the stress-difference-to-failure (SDF) to quantify the proximity of a stress state to either shear or

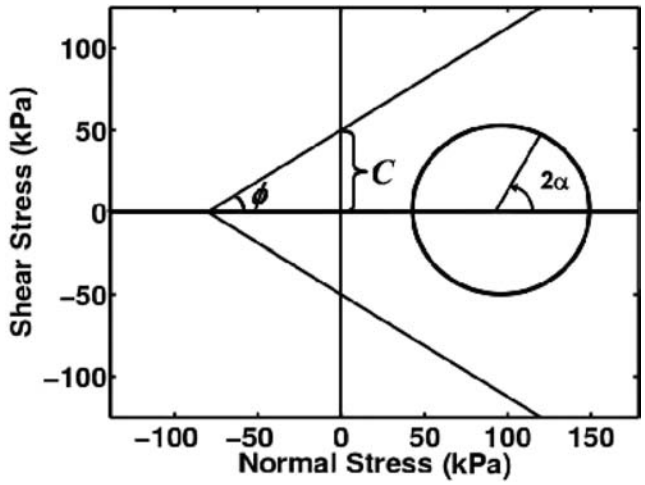

Figure 3. The Mohr circle and Mohr–Coulomb failure envelope. C is the cohesion and ϕ is the internal angle of friction. When failure occurs, α refers to the angle between the normal to the failure plane and the principal stress direction corresponding to the most compressive stress, σ_1.

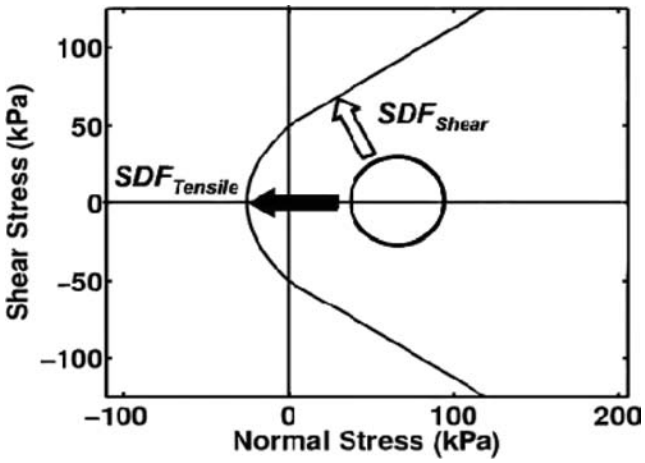

Figure 4. The Mohr circle and modified Griffith failure envelope. The dark arrow displays how far the circle is from failing in tension indicated by the Griffith portion of the envelope. The white arrow displays the distance the circle is to failing in shear indicated by the Coulomb portion of the envelope.

tensile failure. A stable stress state is represented by negative values of SDF. Failure takes place when either $\mathrm{SDF}_{\mathrm{shear}}$ or $\mathrm{SDF}_{\mathrm{tensile}}$ is equal to zero, whichever occurs first. The equations to calculate SDF for the modified Griffith envelope are given by (Bourne & Willemse 2001)

$$\mathrm{SDF}_{\mathrm{shear}} = \left(\frac{\sigma_1 - \sigma_3}{2}\right) - \left(\frac{\sigma_1 + \sigma_3}{2}\right)\sin(\phi) - c\cos(\phi), \qquad (12)$$

$$\mathrm{SDF}_{\mathrm{tensile}} = \left(\frac{\sigma_1 - \sigma_3}{2}\right) - \left(\frac{\sigma_1 + \sigma_3}{2}\right) - \frac{c}{2} = -\sigma_3 - \frac{c}{2}, \qquad (13)$$

where σ_1 and σ_3 are the maximum and minimum principal stress components, respectively.

When one of these quantities is zero or negative at a point, the material locally fails. This does not necessarily mean that the slope in its entirety fails, because such collective behaviour depends on the presence of defects as well as on the material properties of the slope in regions that fail. Such post-failure material behaviour is not modelled here. The regions where the stress distance to failure is non-negative should thus be viewed as areas where failure has the potential to take place.

5 HOMOGENEOUS SLOPE

We use this stress model to analyse triggered failure in an unsaturated, 26° slope that has a constant density of 2000 kg m^{-3}, c = 10 kPa and $\phi = 32°$. Before propagating a plane wave through the slope, failure of the static slope occurs at a slope angle of 37° (as determined by eqs (12)–(13). When a slope is cohesive, such as in this example, static failure can occur at a slope angle larger than the internal angle of friction.

Even though an S wave generates larger dynamic stresses at the slope surface than does the P wave, our analysis shows that a P wave with the same PGA produces the same type of failure mechanisms at the same depth. Using eqs (12)–(13), the following figures depict a snapshot in time showing the initiation of tensile and shear failure in the slope. Fig. 5 shows $\mathrm{SDF}_{\mathrm{tensile}}$ due to a P wave with an angle of incidence of 30°,with a PGA of 0.1 g. For one instant in time, dynamic stresses are great enough to produce tensile failure shown as the circled region in dark red near the surface of the slope. Negative values of $\mathrm{SDF}_{\mathrm{tensile}}$ in most of the area indicate that the region has not failed in tension. Shear failure, as shown in Fig. 6, takes place at greater depth than tensile failure. There is a limited depth interval for shear failure; the approximate location of shear failure is circled.

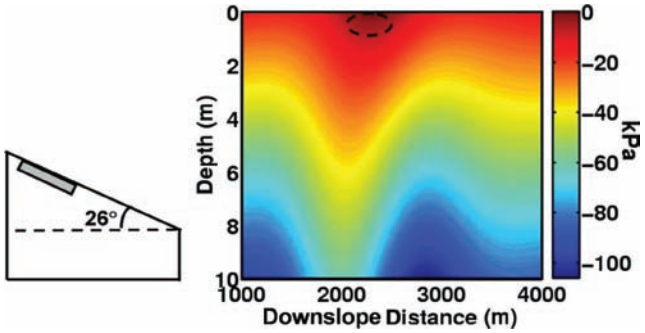

Figure 5. Right-hand panel: $\mathrm{SDF}_{\mathrm{tensile}}$ for a slope of 26° and c = 10 kPa due to a P wave with an incidence angle of 30°, normalized to a PGA = 0.1 g. The shaded area in the left-hand panel shows the region of the slope shown on the right-hand side at a given instant in time. Failure occurs near the free surface, indicated by the circled region. Negative values of $\mathrm{SDF}_{\mathrm{tensile}}$ in the colourbar indicate the amount of stress necessary for tensile failure to occur.

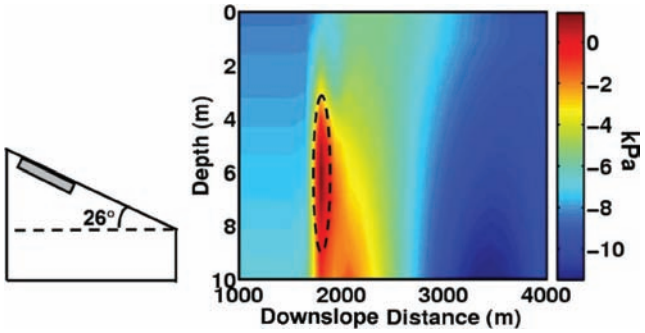

Figure 6. Right-hand panel: $\mathrm{SDF}_{\mathrm{shear}}$ for a slope of 26° and c = 10 kPa due to a P wave with an incidence angle of 30°, normalized to a PGA = 0.1 g. The shaded area in the left-hand panel shows the region of the slope shown on the right-hand side. Initiation of shear failure is located within the dashed line.

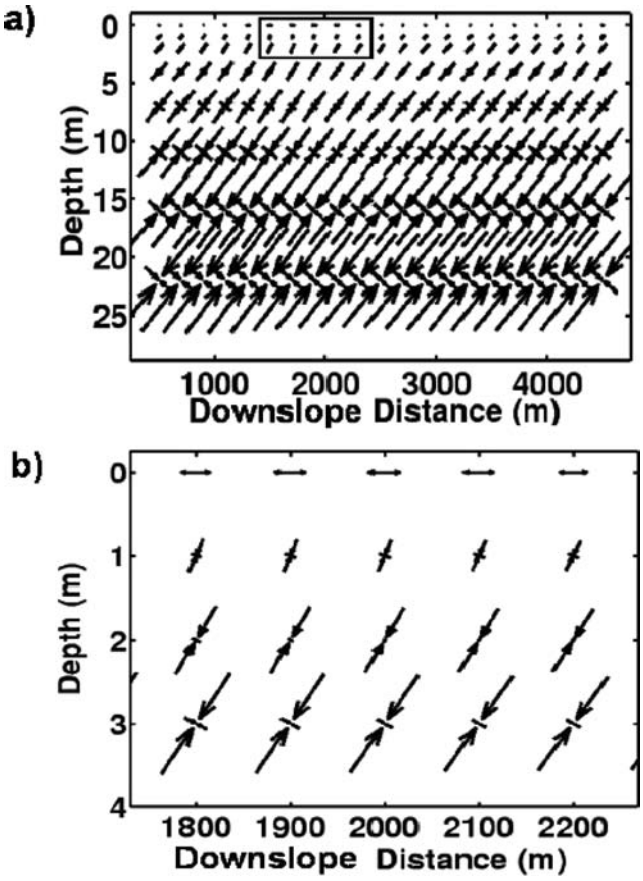

Figure 7. The total principal stress components and directions computed for the 26° slope due to a *P* wave with an incidence angle of 30°, normalized to a PGA = 0.1 g shown in the coordinate system of Fig. 1. Inward arrows represent compression, while outward pointing arrows indicate tension. The box in (a) is enlarged in (b) to show that tensile stress exists to a depth of 1 m and below this depth, the principal stresses are compressive.

Each failure mechanism can be analysed by computing the principal stress components and directions of the sum of the static and dynamic stress. Fig. 7 shows the principal stresses for the 26° slope due to the incident *P* wave at the same instance in time as in Figs 5 and 6. The directions of the arrows indicate principal stress directions while the length represents the magnitude of the principal stress component. Inward pointing arrows represent compression and outward pointing arrows near the surface indicate tension. The stress is tensile near the surface, therefore, the location of the box in (a) is enlarged for clarity in panel (b).

Tensile stress shown in Fig. 7 is limited to the uppermost meter, which is the same location where tensile failure occurs in Fig. 5. At a depth of 3 m, both principal stresses are compressive, hence tensile failure cannot occur at this depth.

To further understand the depths of shear and tensile failure, we derive approximations of the dynamic stresses in terms of the acceleration at the surface, the slowness of the incoming wave, and the dominant frequency. These stress equations follow from Newton's Law and Hooke's Law. The derivation of the approximations for $\sigma_{xx}^{\text{dyneq}}$, $\sigma_{zz}^{\text{dyneq}}$, $\sigma_{xz}^{\text{dyneq}}$ is in Appendix A:

$$\sigma_{xx}^{\text{dyneq}}(z) = \frac{4\mu(\lambda+\mu)}{\lambda+2\mu}\left(\frac{p}{2\pi f}\right)a_x, \tag{14}$$

$$\sigma_{zz}^{\text{dyneq}}(z) = -\rho a_z z, \tag{15}$$

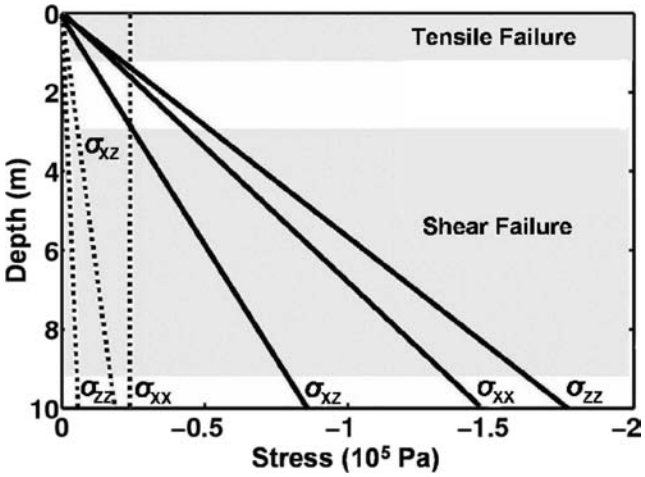

Figure 8. Stress components as a function of depth for the example outlined in Figs 5–6, at a downslope distance of 2000 m. Tensile failure for this 26° slope is indicated by the upper shaded region, while shear failure takes place in the lower shaded region. The dotted lines represent the components of σ^{dyneq}, produced by eqs (14)–(16), which are used in place of σ^{dynamic} with depth. The solid lines represent the components of σ^{static}.

$$\sigma_{xz}^{\text{dyneq}}(z) = -\left\{\rho a_x + \left[\frac{4\mu(\lambda+\mu)}{\lambda+2\mu}\right]\left(\frac{p}{2\pi f}\frac{\partial a_x}{\partial x}\right)\right\}z, \tag{16}$$

where p is the slowness of the incoming wave along the slope, f the peak frequency, a_x the acceleration in the direction parallel to the slope and a_z the acceleration in the direction normal to the slope. Using a first-order Taylor expansion in z these expressions relate the stress in the near-surface to the acceleration at the free surface. Note that the tractions at the free surface vanish, while $\sigma_{xx}^{\text{dyneq}}$ is not a function of z and can be non-zero. Gipprich (2005) shows that these equations are a good approximation to the dynamic stresses produced by the finite-element model by comparing the stress computed from eqs (14) to (16) with those predicted by the finite element model.

We use eqs (14)–(16) to estimate the depth of failure more closely. Fig. 8 shows the static and dynamic stress components as a function of depth for the stress state of Figs 5 and 6 at a downslope distance of 2000 m, which is the distance at which failure takes place. In Fig. 8, we use the dynamic stress eqs (14)–(16) instead of the modelled dynamic stresses with depth. The region of tensile failure is shaded at the near surface, and the region for shear failure is shaded at depth. The tensile failure near the surface is due to $\sigma_{xx}^{\text{dyneq}}$, since the other stress components approach zero near the surface. To further understand what determines the depth of tensile failure, we make the assumption that failure takes place when the dynamic tensile stress $\sigma_{xx}^{\text{dyneq}}$ overcomes the compressive static stress $\sigma_{xx}^{\text{static}}$. We use $\sigma_{zz}^{\text{static}}$ as a proxy for the horizontal compressive stress, because according to expressions (2)–(3) $\sigma_{xx}^{\text{static}}$ is of the same order of magnitude as $\sigma_{zz}^{\text{static}}$. The tensile stress is larger than the compressive stress when

$$\left|\sigma_{xx}^{\text{dyneq}}\right| > \sigma_{zz}^{\text{static}}, \tag{17}$$

substituting the static stress eq. (3) for $\sigma_{zz}^{\text{static}}$ gives

$$\left|\sigma_{xx}^{\text{dyneq}}\right| > \rho g z\cos(\theta), \tag{18}$$

and solving for the estimated depth of failure,

$$z < \frac{\left|\sigma_{xx}^{\text{dyneq}}\right|}{\rho g\cos(\theta)}. \tag{19}$$

At the point of failure, for the particular case outlined above, the tensile stress is equal to the tensile strength of the slope. Because $\sigma_{xx}^{\text{dyneq}}$ is constant with depth, and is the only source of stress causing tensile failure, its value at failure is approximately equal to tensile strength, represented by $c/2$,

$$\left|\sigma_{xx}^{\text{dyneq}}\right| \approx \frac{c}{2}, \tag{20}$$

and substituting this into eq. (19) gives:

$$z < \frac{c}{2\rho g \cos(\theta)}. \tag{21}$$

Therefore, the estimated depth of tensile failure depends on the tensile strength of the slope, and varies with density and slope angle. For this example, $c = 10$ kPa, $\rho = 2000\ \text{kg m}^{-3}$ and $\theta = 26^\circ$ and from (21) the depth of tensile failure is $z < 0.3$ m.

This analysis provides an estimate of the maximum depth of tensile failure without having to analyse $\text{SDF}_{\text{tensile}}$. As $\sigma_{xx}^{\text{dyneq}}$ is constant with depth and the absolute value of the static stresses increase with depth, tensile failure does not occur at greater depth due to the growth of the compressive, static stress components with depth.

As shown in Fig. 8, shear failure takes place when all static stress components are larger than the corresponding dynamic stresses. Shear failure occurs at a depth when the smallest static stress component $\sigma_{xz}^{\text{static}}$ is approximately equal to the largest dynamic stress, $\sigma_{xx}^{\text{dyneq}}$:

$$\sigma_{xx}^{\text{dyneq}} \approx \sigma_{xz}^{\text{static}}. \tag{22}$$

For this particular situation, substituting the static stress eq. (4) for $\sigma_{xz}^{\text{static}}$ gives:

$$\sigma_{xx}^{\text{dyneq}} \approx \rho g z \sin(\theta), \tag{23}$$

and solving for depth,

$$z \approx \frac{\sigma_{xx}^{\text{dyneq}}}{\rho g \sin(\theta)}. \tag{24}$$

The depth of failure can be found by substituting dynamic stress eq. (14) for $\sigma_{xx}^{\text{dyneq}}$,

$$z \approx \frac{\frac{4\mu(\lambda+\mu)}{\lambda+2\mu}\left(\frac{p}{2\pi f}\right)a_x}{\rho g \sin(\theta)}. \tag{25}$$

The input parameters for this example are $\lambda = 5.0 \times 10^8$ Pa, $\mu = 5.0 \times 10^9$ Pa, $p = 0.000289\ \text{s m}^{-1}$, $f = 1.0$ Hz and $a_x = 0.3\ \text{m s}^{-2}$. Given this information, the depth of initial shear failure is about $z = 3$ m. Eq. (25) demonstrates that the depth of shear failure depends on several factors that include the PGA, as well as the horizontal slowness of the incoming wave (p).

This homogeneous slope analysis allows us to relate the depths of shear and tensile failure in the slope to the dependence of the dynamic stresses with depth. Statically, the entire slope at 26° is stable, but when a plane wave is incident on the slope, in the near-surface, it is the $\sigma_{xx}^{\text{dyneq}}$ component of stress that causes tensile failure in the x-direction. Deeper within the slope, $\sigma_{xx}^{\text{dyneq}}$ is the largest dynamic stress component, but smaller than the static stresses. When each principal stress component of the total stress is positive, tensile failure can no longer take place. We see in eqs (14)–(16) that the dynamic stress state accounts for both the horizontal and vertical components of the PGA, while the static stress eqs (2)–(4) are related to gravitation al acceleration. Therefore, when the PGA is normalized to a value less than the gravitational acceleration, such as in this example, the static stress components eventually become larger than the dynamic stress components at depth. At a depth where dynamic stresses are small in comparison to static stresses, the dynamic stress state has little influence on the total stress field and no longer triggers failure, which in this example, takes place at a depth near 9 m.

6 LAYERED SLOPE

Terzaghi *et al.* (1996) characterize a layered slope as a simple two-layer medium consisting of an upper layer representing a weak, weathered zone overlying rock. We follow this description by focusing on the failure analysis of an unsaturated slope with two layers parallel to the surface. In our analysis, the upper 5 m represent a weathered layer overlying a stronger, sedimentary layer. The shallow layer has P- and S-wave velocity α_1 and β_1, respectively, density ρ_1, internal friction angle ϕ_1, and cohesion c_1, that are smaller than those for the stronger layer, α_2, β_2, ρ_2, ϕ_2 and c_2. The values used in the layered and homogeneous models are shown in Table 1. The weathered layer has the same values of cohesion and internal angle of friction as the homogeneous model, so that we can compare failure in the upper meters of the slope, where tensile failure is found. We use this model to investigate the influence of the amplification of the wave in the near-surface layer on slope failure.

The interface between the two layers is a solid/solid boundary. An incoming wave that hits this interface produces a different set of reflected and transmitted waves than for the homogeneous model. According to Snell's law, the slope-parallel slowness of the incident wave remains the same while crossing the interface between layers during the reflection/transmission process (Aki & Richards 2002). Because the upper layer has velocities less than the sedimentary layer, the angles of the transmitted waves in the upper layer are less than those of the reflected P and S waves in the lower layer.

Our analysis for this model shows that conditions in the layered slope produce tensile failure in the upper meters of the slope and shear failure a few meters deeper within the upper and lower layers. For the layered model, we show the stress difference to shear and tensile failure produced by an S wave with an incidence angle of 30°, normalized to a PGA of 0.1 g in Figs 9 and 10. These figures show that there are two distinct locations of failure, each having a different mechanism of failure. In the two-layer model, failure takes place at shallower slopes compared with the homogeneous case. Shear and tensile failure take place in the layered medium for a slope of 19°. The weathered layer initially fails in tension near the surface down to a depth of 1 m. Below the interface, failure only occurs at 6 m depth, which is in shear. For the tests completed and examples demonstrated in this paper, we find that given the same failure criteria, the locations of the failure mechanisms in the layered

Table 1. Parameter values used in the slope models.

Model	α (m s^{-1})	β (m s^{-1})	ρ (kg m^{-3})	ϕ (°)	c (kPa)
Homogeneous	1730	500	2000	32	10
Layered: low velocity	1500	800	1500	32	10
Layered: sedimentary	2200	1000	2200	40	50

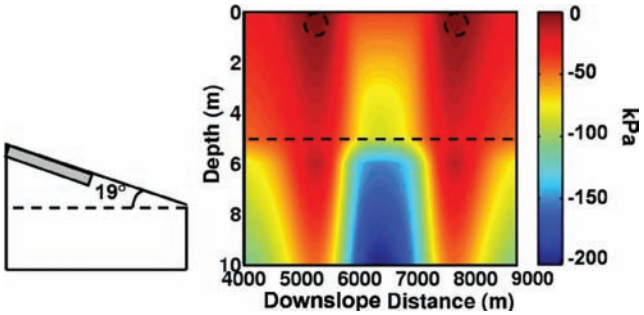

Figure 9. Right-hand panel: SDF $_{\text{tensile}}$ for a layered slope of 19° due to an *S* wave with an incidence angle of 30°, normalized to a PGA = 0.1 g. The upper layer contains $c = 10$ kPa while the lower layer has $c = 50$ kPa. The boundary between the two layers is indicated by the dashed line. The shaded area in the left-hand panel shows the region of the slope shown on the right-hand side. Tensile failure occurs at the near surface, indicated by the circled regions.

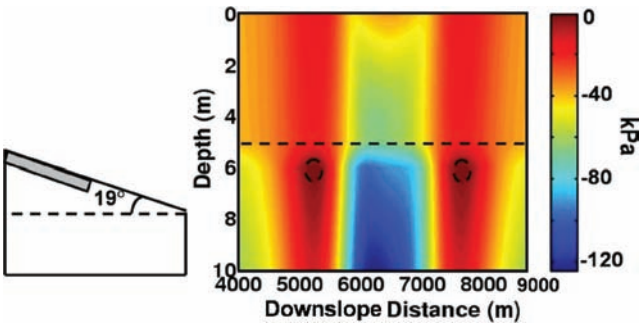

Figure 10. Right-hand panel: SDF $_{\text{shear}}$ for a layered slope of 19° due to an *S* wave with an incidence angle of 30°, normalized to a PGA = 0.1 g. The upper layer contains $c = 10$ kPa while the lower layer has $c = 50$ kPa. The boundary between the two layers is indicated by the dashed line. The shaded area in the left-hand panel shows the region of the slope shown on the right-hand side. The initiation of shear failure is circled at 6 m depth.

slope resemble those in the homogeneous slope. This is largely due to the fact that the presence of the layer has little impact on the dynamic stresses in the near surface because the wavelength of the incoming wave (800 m) is much larger than the depth of the upper layer (5 m).

7 DISCUSSION

We provide a model for the role of shear and tensile failure in the seismic triggering of landslides. This model explains the initiation of tensile failure in the near-surface (upper meters) and shear failure at depth in a slope subject to dynamic stresses, and provides a useful perspective on how seismic shaking triggers slope failure. For specific slope conditions we can test the susceptibility to both shear and tensile failure due to varying dynamic stresses. This modelling approach is an improvement over existing approaches that only consider shear failure and do not account for tensile failure. If dynamic stresses from an earthquake can be measured or estimated, our modelling can be implemented to provide insight into the generation of slope failure and to create a more complete dynamic model than has been previously possible.

Fig. 11 summarizes the estimates of the depth ranges for shear and tensile failure that we derived in Section 4 and that is confirmed by the numerical simulations shown in Figs 5, 6, 9 and 10. Fig. 11 suggests a plausible scenario in which shallow tensile failure combines with deeper shear failure to cause a slope to fail . As stresses build, tensile (or shear) failure initiates, inducing shear (or tensile) failure. Our model examines only one simple dynamic stress condition and deeper failures do occur during earthquakes, although these failures are most likely triggered by other, more complex stress conditions that we have not modelled. We are unable to determine from our model which type of failure might occur first in a slope because our analysis based on linear theory can not account for the details of the post-failure process, but Fig. 11 illustrates how shear and tensile failure may collaborate to cause slope failure.

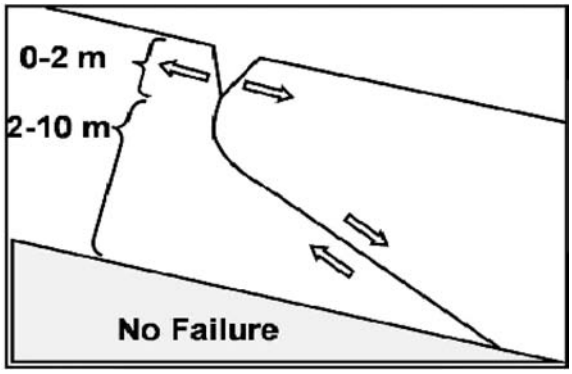

Figure 11. The two mechanisms of failure that occur and collaborate to create slope failure. Tensile failure occurs in the upper meters near the surface, while shear failure takes place at greater depth, below which, failure does not occur.

ACKNOWLEDGMENTS

We thank Fred Witham and an anonymous reviewer for their clear and constructive comments. This work was supported by the National Earthquake Hazards Reduction Program (NEHRP) of the U.S. Geological Survey through award #04HQGR0108. We extend our thanks to Dr Matthew Haney for providing his finite-element code.

NOTATION

σ^{static}	Static stress components
σ^{dynamic}	Dynamic stress components produced by the model
σ^{dyneq}	Dynamic stress components produced by equations
c	Cohesion
ϕ	Internal angle of friction
λ	Lamé elastic constant
μ	Lamé elastic constant
ρ	Density
θ	Slope angle
p	Slowness of a plane wave along the slope
i_p, i_s	Angle of incidence for *P* and *S* waves
f and ω	Frequency and angular frequency
u_x	Component of displacement parallel to slope
u_z	Component of displacement perpendicular to slope
v_x	Component of velocity parallel to slope
v_z	Component of velocity perpendicular to slope
a_x	Component of acceleration parallel to slope
a_z	Component of acceleration perpendicular to slope
τ	Shear stress
σ	Normal stress
σ_{ij}	Stress tensor
σ_1, σ_3	Largest and smallest principal stress components.

REFERENCES

Aki, K. & Richards, P.G., 2002. *Quantitative Seismology*, 2nd edn, University Science Books, Sausalito, CA.

Bourne, S.J. & Willemse, E.J., 2001. Elastic stress control on the pattern of tensile fracturing around a small fault network at Nash Point, UK, *J. Struct. Geol.,* **23,** 1753–1770.

Brace, W.F., 1960. An extension of the Griffith theory of fracture to rocks, *J. geophys. Res.*, **65**, 3477–3480.

Bray, J.D. & Rathje, E.M., 1998. Earthquake-induced displacements of solid-waste landfills, *J. Geotech Geoenviron. Eng.*, **124**, 242–253.

Das, B.M., 1997. *Advanced Soil Mechanics*, 2nd edn, Taylor and Francis, Washington, DC.

Gipprich, T.L., 2005. The role of shear and tensile failure in dynamically triggered landslides, *Master's thesis*, Colorado School of Mines, http://www.mines.edu/~rsnieder/Tamarathesis.pdf.

Haney, M.M., 2004. An investigation of sealing and episodic pulsing of fluids at a minibasin-bounding growth fault from seismic reflection images, *PhD thesis*, Colorado School of Mines.

Harp, E.L., Wilson, R.C. & Wieczorek, G.F., 1981. Landslides from the February 4, 1976, Guatemala earthquake, *U.S. Geological Survey Professional Paper*, 1204-A.

Jaeger, J.C. & Cook, N.G., 1976. *Fundamentals of Rock Mechanics*, John Wiley and Sons, Inc., New York.

Jibson, R.W., 1993. Predicting earthquake-induced landslide displacements using Newmark's sliding block analysis, *Transport. Res. Rec.* **1411**, 9–17.

Jibson, R.W., Harp, E.L. & Michael, J.A., 2000. A method for producing digital probabilistic seismic landslide hazard maps, *Eng. Geol.*, **58**, 271–289.

Jibson, R.W., Harp, E.L., Schultz, W. & Keefer, D.K., 2004. Landslides triggered by the 2002 m-7.9 Denali Fault, Alaska, earthquake and the inferred nature of the strong shaking, *Earthq. Spectra*, **20**, 669–691.

Mello, U.T. & Pratson, L.F., 1999. Regional slope stability and slope-failure mechanics from the two-dimensional state of stress in an infinite slope, *Mar. Geol.*, **154**, 339–356.

Middleton, G.V. & Wilcock, P.R., 1994. *Mechanics in the Earth and Environmental Sceinces*, Cambridge University Press, Cambridge, UK.

Newmark, N.M., 1965. Effects of earthquakes on dams and embankments, *Geotechnique*, **15**, 139–160.

Rathje, E.M. & Bray, J.D., 1999. An examination of simplified earthquake-induced displacement procedures for earth structures, *Can. Geotech. J.*, **36**, 72–87.

Rathje, E.M. & Bray, J.D., 2000. Nonlinear coupled seismic sliding analysis of earth structures, *J. Geotech. Geoenviron. Eng.*, **127**, 1002–1014.

Savage, W.Z. & Swolfs, H.S., 1992. Near-surface crustal stresses—theory and application, *Trends Geophys. Res.*, **1**, 217–250.

Selby, M.J., 1993. *Hillslope Materials and Processes*, 2nd edn, Oxford University Press, Oxford.

Sitar, N. & Clough, G.W., 1983. Seismic response of steep slopes in cemented soils, *ASCE J. Geotech. Eng.*, **109**, 210–227.

Terzaghi, K., 1950. Mechanics of landslides, *Application of Geology to Engineering Practice*, Geological Society of America, pp. 83–123.

Terzaghi, K., Peck, R.B. & Msri, G., 1996. *Soil Mechanics in Engineering Practice*, 3nd edn, John Wiley and Sons, Inc., New York.

APPENDIX A: DERIVATION OF DYNAMIC STRESS EQUATIONS FROM PLANE WAVE SOLUTIONS

Newton's Law and Hooke's Law are, in the frequency domain, given by

$$-\rho\omega^2 u_x = \frac{\partial \sigma_{xx}}{\partial x} + \frac{\partial \sigma_{xz}}{\partial z}, \tag{A1}$$

$$-\rho\omega^2 u_z = \frac{\partial \sigma_{xz}}{\partial x} + \frac{\partial \sigma_{zz}}{\partial z}, \tag{A2}$$

$$\sigma_{xx} = (\lambda + 2\mu)\frac{\partial u_x}{\partial x} + \lambda\frac{\partial u_z}{\partial z}, \tag{A3}$$

$$\sigma_{zz} = \lambda\frac{\partial u_x}{\partial x} + (\lambda + 2\mu)\frac{\partial u_z}{\partial z}, \tag{A4}$$

$$\sigma_{xz} = \mu\left(\frac{\partial u_z}{\partial x} + \frac{\partial u_x}{\partial z}\right), \tag{A5}$$

where u is the displacement and ω the angular frequency. At the surface, $\sigma_{zz}(z = 0) = \sigma_{xz}(z = 0) = 0$. We want to find the stress near the free surface and express this in terms of acelleration at the free surface. The z-derivative of displacement is non-zero but cannot be measured, therefore, we eliminate $\partial u_z/\partial z$ from (A3) to (A4) by taking $(\lambda + 2\mu)$(A3) $-$ (λ)(A4):

$$(\lambda + 2\mu)\sigma_{xx} - \lambda\sigma_{zz} = \left[(\lambda + 2\mu)^2 - \lambda^2\right]\frac{\partial u_x}{\partial x}. \tag{A6}$$

At the surface, $\sigma_{zz} = 0$, hence,

$$\sigma_{xx}^{(0)} = \frac{4\mu(\lambda + \mu)}{\lambda + 2\mu}\frac{\partial u_x}{\partial x}, \tag{A7}$$

where $\sigma_{ij}^{(0)}$ refers to the stress at the surface of the slope. Using a Taylor series expansion, $\sigma_{xx}(z) = \sigma_{xx}^{(0)} + O(z)$. The first term gives the dominant contribution of σ_{xx} near the surface, which is expression (A7) in this approximation.

Since $\sigma_{zz}^{(0)} = 0$,

$$\sigma_{zz}(z) = \frac{\partial \sigma_{zz}^{(0)}}{\partial z}z + O(z^2). \tag{A8}$$

$\partial\sigma_{zz}^{(0)}/\partial z$ is found by evaluating (A2) at $z = 0$, where σ_{xz} vanishes at the free surface, hence

$$-\rho\omega^2 u_z^{(0)} = \frac{\partial \sigma_{zz}^{(0)}}{\partial z}. \tag{A9}$$

Inserting this into (A8) gives:

$$\sigma_{zz}(z) = -\rho\omega^2 u_z^{(0)} z + O(z^2). \tag{A10}$$

Similarly,

$$\sigma_{xz}(z) = \frac{\partial \sigma_{xz}^{(0)}}{\partial z}z + O(z^2). \tag{A11}$$

Substituting (A7) into (A1) to evaluate this derivative at the free surface gives,

$$-\rho\omega^2 u_x = \left\{\frac{\partial}{\partial x}\left[\frac{4\mu(\lambda + \mu)}{\lambda + 2\mu}\frac{\partial u_x}{\partial x}\right]\right\} + \frac{\partial \sigma_{xz}}{\partial z}, \tag{A12}$$

$$\frac{\partial \sigma_{xz}}{\partial z} = -\rho\omega^2 u_x - \left\{\frac{\partial}{\partial x}\left[\frac{4\mu(\lambda + \mu)}{\lambda + 2\mu}\frac{\partial u_x}{\partial x}\right]\right\}. \tag{A13}$$

Therefore, the dynamic stress equations for the near-surface are to leading order given by:

$$\sigma_{xx}^{\text{dyneq}}(z) = \frac{4\mu(\lambda + \mu)}{\lambda + 2\mu}\frac{\partial u_x^{(0)}}{\partial x} + O(z), \tag{A14}$$

$$\sigma_{zz}^{\text{dyneq}}(z) = -\rho\omega^2 u_z^{(0)} z + O(z^2), \tag{A15}$$

$$\sigma_{xz}^{\text{dyneq}}(z) = -\left\{\rho\omega^2 u_x^{(0)} + \frac{\partial}{\partial x}\left[\frac{4\mu(\lambda + \mu)}{\lambda + 2\mu}\frac{\partial u_x^{(0)}}{\partial x}\right]\right\}z + O(z^2). \tag{A16}$$

Considering plane wave solutions, the displacement is given by:

$$u(x, z, t) = u(t - px, z), \tag{A17}$$

where p is the slowness or ray parameter. Therefore, the x-derivative of displacement is given by:

$$\frac{\partial u_x}{\partial x} = -p\frac{\partial u_x}{\partial t} = -pv_x, \tag{A18}$$

where v_x is the particle velocity in the x-direction. In the following we consider harmonic motion with frequency f. Using eq. (A18) for such motion and expression

$$v(\omega) = \frac{a(\omega)}{-i\omega}, \tag{A19}$$

that relates velocity to the acceleration, eq. (A18) can be written as:

$$\frac{\partial u_x}{\partial x} = \frac{-p}{-i\omega}a_x = \frac{p}{2\pi i f}a_x, \tag{A20}$$

where a_x is acceleration, $i = \sqrt{-1}$, and f the frequency of the wave. The absolute value of the derivative of displacement is approximately equal to:

$$\left|\frac{\partial u_x}{\partial x}\right| \approx \left|\frac{p}{2\pi f}a_x\right|. \tag{A21}$$

The slowness, p, is also related to the angles of incidence, i_p and i_s, and the velocities at the surface, v_p and v_s, of the P and S waves, respectively,

$$p = \frac{\sin(i_p)}{v_p} = \frac{\sin(i_s)}{v_s}. \tag{A22}$$

By substituting (A21) for the derivative of displacement in eqs (A14)–(A16), the stress components are related to slowness and, hence, the angle of incidence of a plane wave,

$$\sigma_{xx}^{\text{dyneq}}(z) = \frac{4\mu(\lambda+\mu)}{\lambda+2\mu}\left(\frac{p}{2\pi f}\right)a_x + O(z), \tag{A23}$$

$$\sigma_{zz}^{\text{dyneq}}(z) = -\rho a_z z + O(z^2), \tag{A24}$$

$$\sigma_{xz}^{\text{dyneq}}(z) = -\left\{\rho a_x + \left[\frac{4\mu(\lambda+\mu)}{\lambda+2\mu}\right]\left(\frac{p}{2\pi f}\frac{\partial a_x}{\partial x}\right)\right\}z + O(z^2). \tag{A25}$$